Licenciat Thesis

Stockholm
January 13, 1998

A measurement of the inclusive branching ratios of τ decays in the Delphi detector at LEP

Kerem Cankoçak

Abstract

In this thesis a report is given on hardware work done on the DELPHI detector and a measurement of the inclusive branching ratios of τ decays. A sample of 16454 $Z \to \tau^+\tau^-$ events collected by the DELPHI experiment at LEP in 1992 is used to measure the inclusive branching ratios of τ decays. The results are

B($\tau \to$ 1 charged particle) = 84.38 $\pm$ 0.27 $\pm$ 0.35 %,
B($\tau \to$ 3 charged particles) = 14.90 $\pm$ 0.27 $\pm$ 0.23% and
B($\tau \to$ 5 charged particles) = 0.51 $\pm$ 0.12 $\pm$ 0.11%.

To be presented on the 9:th of Feb 1998 at 13.15,
Room 4731, Fysikum, Vanadisvägen 9, Stockholm.

Examiner:	Prof. S.-O. Holmgren
Supervisor:	Doc. Klas Hultqvist
Opponent:	Doc. Torbjörn Moa

Publications

Publication I

P. Bambade, A. Benvenuti, M. Boldini, B. Buisson, K. Cankoçak, G. Dubois Dauphin, Ch. De La Vaissiere, V. Giordano, P. Gunnarsson, D. Imbault, A. Jouenne, F. Kapusta, P. Laloux, J. Lesueur, L. Maselli, A. Morelli, P. Rebecchi, M. Rebut, J. Renaud, K. Truong , *Test and Installation of the* 40^o *Counters during the 1993/1994 Shut Down*, DELPHI note 94-48 HERM 1, 5 May 1994.

Publication II

K. Cankoçak, P. Andersson, A. Benvenuti, P. Rebecchi, S. Holmgren, *Study of the* 40^o *Counters in a test beam 1993/1994 Shut Down*, DELPHI note 95-152 CAL-127, 3 Oct 1995.

Publication III

Bell, W., Bonivento, W., Cankoçak, K., Cattai, A., Contri, R., De Min, A., Gorn, L., Navarria, F.L., Ragazzi, S., Szczekowsky, M., Tabarelli de Fatis, T. and Tonazzo, A., *Performance of an artificially aged module of the DELPHI HPC calorimeter*, Nucl.Instr.& Meth. **A378**, Issue 3, (1996) 499.

Contents

Publications **0**

1 Introduction **1**

2 The Experimental Apparatus **1**
2.1 The LEP Collider at CERN 1
2.2 The DELPHI detector 2
2.2.1 The Barrel tracking Detectors 2
2.2.2 The Barrel Electromagnetic Calorimeter 4

3 Improvement of the Hermeticity **4**
3.1 The 40° scintillator counters 5
3.2 Testing the counters 5
3.3 The efficiency and Performance of the counters 6

4 $\mathcal{T}$ lepton physics **9**
4.1 τ production in $\mathrm{e^+e^-} \to Z \to \tau^+\tau^-$ 10

5 Selection of $\tau^+\tau^-$ events in DELPHI **12**
5.1 Event Selection 12
5.1.1 Selection Efficiency 16
5.1.2 Background 16

6 Migration of Topologies **17**

7 Comparison of the Migration Matrix **18**

8 Reconstruction problems and corrections **19**

9 The Inclusive branching Ratio Measurements **20**

10 Conclusion **21**

Acknowledgments **23**

References **24**

1 Introduction

Since its discovery in 1975 [1], the fundamental properties of the τ lepton have been measured, including the many decay modes and the corresponding branching ratios. Being the heaviest lepton, τ decays via weak interaction into lighter leptons sometimes accompanied by hadrons. One interesting aspect of τ decay physics is the "inconsistency" which was observed between the τ topological branching ratios and the τ exclusive branching ratios in the early measurements [2]. In the topological branching ratio measurements, τ decays are classified according to their charged track topology (1, 3, 5 tracks), whereas in the exclusive measurements, the final decay product is identified explicitly ($\tau \to e\nu\bar{\nu}$, $\tau \to \mu\nu\bar{\nu}$, $\tau \to 3\pi\nu$, etc.). The topological branching ratio of τ decay into one charged track should be equal to the sum of the exclusive branching ratios which have one charged track, like $\tau \to e\nu\bar{\nu}$, $\tau \to \mu\nu\bar{\nu}$, etc., and so on for the other decay modes. The discrepancy between the topological and the exclusive branching ratios of the one charged particle decay mode of τ , the so-called "missing modes problem", has created an interest over some years. With more recent measurements from LEP, such as those described in this note, together with new measurements of the tau-mass [3] and lifetime [4] a much more consistent picture of the tau decay properties has emerged [5, 6].

The tau lepton is abundantly produced in $\mathrm{e^+e^-}$ collisions at LEP through the decay of Z bosons. In this analysis we examined the topological branching ratios of the τ lepton into one charged particle (B_1), three charged particles (B_3) and five charged particles (B_5) in addition to neutrals, using an event sample of 16454 $Z \to \tau^+\tau^-$ decays, collected in the barrel region of the DELPHI detector. The events were recorded at the Z peak and correspond to an integrated luminosity of $21.87\mathrm{pb}^{-1}$ during the running period of 1992.

2 The Experimental Apparatus

The Large Electron Positron collider (LEP) started operation in August 1989 at CERN. LEP accelerates electrons and positrons in opposite directions in a vacuum pipe before inducing them to collide. The LEP collider's initial energy was chosen to be around 91 GeV to measure precisely the Z boson properties. The theory of fundamental particles known as the "Standard Model" [11] has been critically tested by studying the decays of Z.

In a second step, the LEP energy has been increased by the installation of superconducting RF cavities, and has reached 183 GeV in 1997. The physics motivations for this energy upgrade were mainly the study of W^+W^- production and the search for new particles.

2.1 The LEP Collider at CERN

With a circumference of 26.7 km, LEP is the largest accelerator to date. The four LEP experiments ALEPH, DELPHI, OPAL and L3 are situated in the accelerator ring about 100 m below ground. The electrons and positrons are injected into the LEP collider after being accelerated by a series of other accelerators. The beams are accelerated first in two linear accelerators (LINAC) up to 600 GeV and then injected into the Electron Positron Accumulating ring (EPA) where they are accumulated and cooled by synchrotron radiation. They are then injected into the first Proton Synchrotron (PS) built at CERN, where they are accelerated up to 3.5 GeV. Then, they are sent to the Super Proton Synchrotron (SPS) to be accelerated up to 20 GeV. Finally, bunches of electrons and positrons are transferred into the LEP ring, as shown in Fig. 1.

LEP consists of a single almost circular ring, with eight arcs. Electrons and positrons are maintained on a circular orbit by dipole magnets installed in the arcs. The beams are focussed by quadrupole magnets positioned both along the straight sections and in the arcs of the ring. The collisions of the e^+e^- beams takes place at the centres of straight sections in-between the arcs.

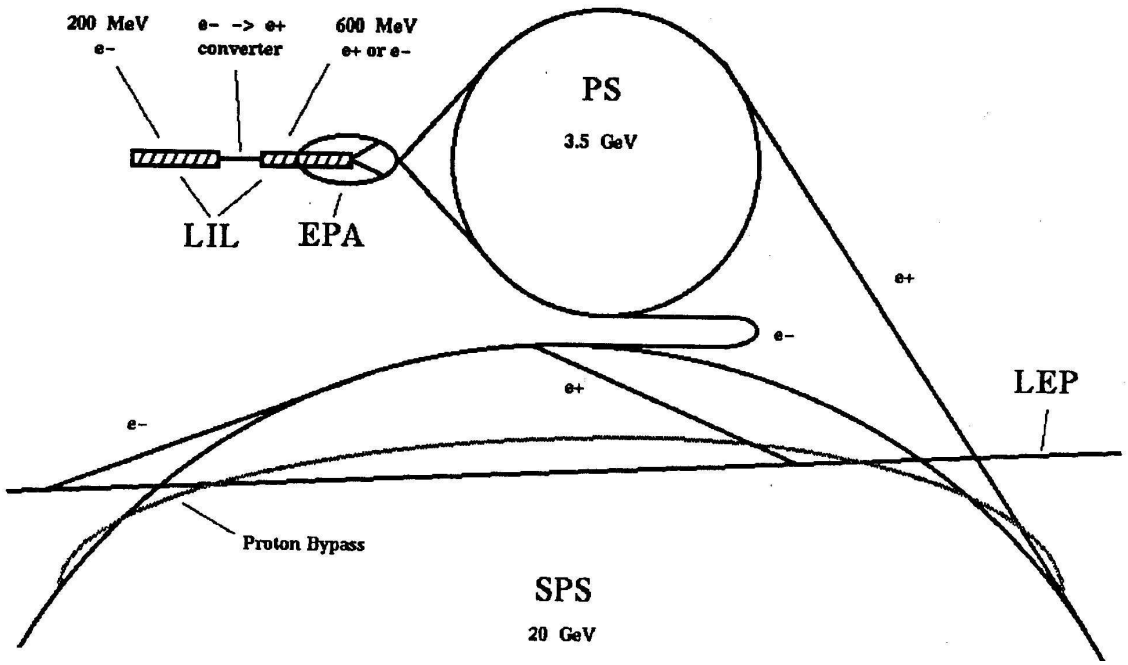

Figure 1: Schematic view of the LEP injection system. Electrons and positrons accelerated in LEP Injector Linacs (LIL) are then injected into the Electron Positron Accumulator (EPA). They are then injected first to the Proton Synchrotron (PS) and later to the Super Proton Synchrotron (SPS) and then finally into the LEP ring itself.

2.2 The DELPHI detector

DELPHI (Detector with Lepton, Photon and Hadron identification) is one of the four large scale detectors each installed around one of the interaction points of LEP. The operation of the detector is the result of a common effort of many hundreds of physicists and technicians. Electron and positron beams are accelerated in the LEP ring and collided at an energy close to 91 GeV in the centre-of-mass, producing Z particles of which several million decays have now been collected. The Delphi detector is described extensively in [12]. We will concentrate on the parts used for this analysis which are mainly VD, ID, TPC, OD, HPC and MUB.

2.2.1 The Barrel tracking Detectors

In the barrel region of the detector, tracking is done with the Vertex Detector (VD), the Inner Detector (ID), the Time projection Chamber (TPC), the Outer Detector (OD) and the Barrel Muon

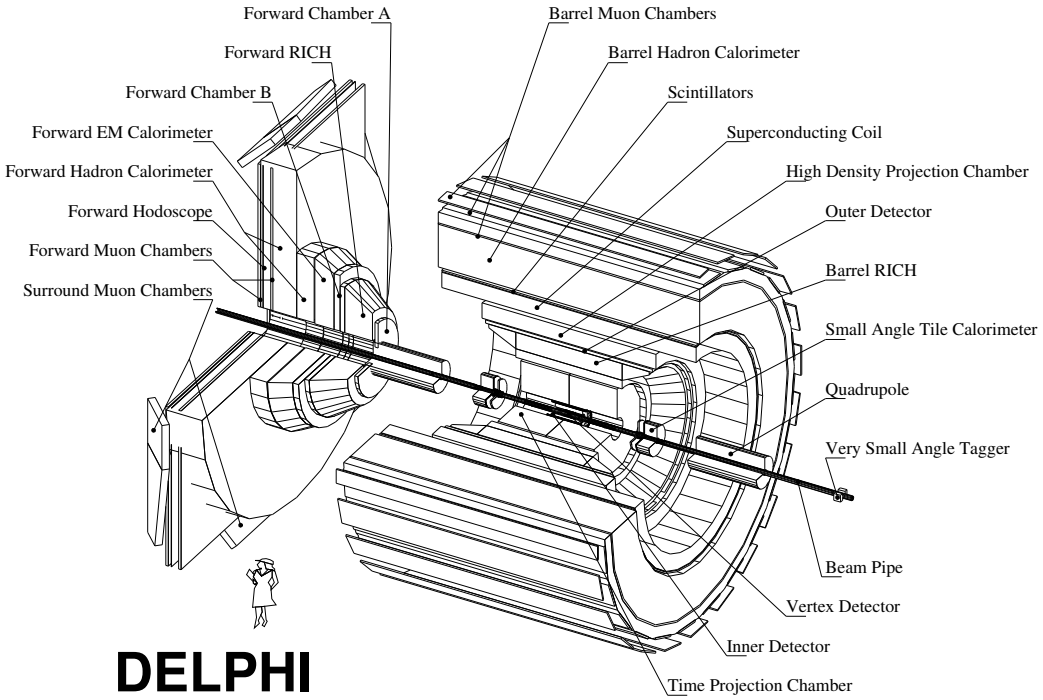

Figure 2: The DELPHI detector at LEP.

Chambers (MUB). The vertex detector (VD) is the one nearest to the collision point and it consists of three layers of silicon strip detectors at radii of 6.3, 9 and 11 cm. Each VD layer has 24 sectors in azimuthal angle ϕ around the beam and 4 segments in z (along the e^- beam). The VD covers the polar angle of $44° < \theta < 136°$ (increased to $25° < \theta < 155°$, in 1994 [14]). It has an Rϕ resolution around 11 μm and a z resolution around 13 μm. This detector provides precise extrapolation of the tracks back towards the interaction point.

The Inner Detector (ID) provides intermediate precision position and trigger information. The inner drift chamber of the ID has a jet-chamber geometry with 24 azimuthal sectors, each providing up to 24 $R\phi$ points per track. The surrounding jet-chamber consist of 5 cylindrical MWPC (MultiWire Proportional Chamber) layers giving Rz information, used in triggering, but also in resolving the left/right drift ambiguities inherent in the jet-chamber. In 1995 these layers were replaced by straw tubes. The polar angle coverage of the detector is $30° < \theta < 150°$. The two track resolution is about 1mm.

The Time Projection Chamber (TPC) is the principal tracking device of DELPHI. Providing the dE/dX information, TPC helps in particle identification as well. It has six sectors in ϕ and two segments along z. At the end of each sector and segment there is a MWPC. The charge deposited by the tracks drifts through the gas volume along z to the end-plates. Each MWPC has 192 sense wires and 16 circular pad rows. The TPC covers the polar angle region $20° < \theta < 160°$. The resolution is about 150 μm in Rϕ and 600 μm in z.

The Outer Detector (OD) provides a final precise position and direction measurement with a long lever arm. It consists of 5 layers of drift tubes, giving full azimuthal coverage. Three layers are equipped to read the z coordinate by timing the signals at the ends of the anode wires. It covers the polar angle of $42° < \theta < 138°$. The single point precision of $\sigma_{R\phi}$ = 110 μm while

the precision in the z coordinate is σ_z = 3.5 cm.

The Barrel Muon Chambers (MUB) are the farthest from the collision point, since muons can traverse the detector material essentially unaffected. Muons with an energy above 2 GeV can penetrate to the Muon Chambers. MUB covers the polar angle of $53° < \theta < 88°$ and the measurements of resolution on extrapolated tracks give an accuracy of 4 mm in $\sigma_{R\phi}$, 2.5 cm in σ_z.

2.2.2 The Barrel Electromagnetic Calorimeter

The DELPHI High-density Projection Chamber (HPC) represents one of the first large-scale applications of the time projection principle to gas sampling calorimetry. The detector consists of 144 independent modules, arranged in a cylinder with 6 rings (in z) of 24 modules (in ϕ) each. Each HPC module is a trapezoidal box with a width ranging from 52 cm to 64 cm and a depth of 47 cm. The length (along z) is 90 cm, except for modules in the first and last rings which are somewhat shorter. The box is filled with 41 layers of lead separated by gas gaps. An electromagnetic particle showers in the lead and ionizes the gas. The charge drifts along the z direction until it reaches the end of the module where it is collected by a proportional chamber (MWPC) with pad readout. Each MWPC consist of 128 pads arranged in 9 rows, with a scintillator plane for the first level trigger replacing the gas between the second and third row. The number of readout channels in the HPC amounts to 18,432. Being a barrel detector, HPC covers polar angles of $40° \leq \theta \leq 140°$. It is located between 208 cm and 260 cm in r and $\pm$ 254 cm in z. The HPC is a highly granular detector ($1°$ in ϕ) having an energy resolution $\sigma(E)/E = 0.043 + 0.32/\sqrt{E}$ (E in GeV) and a spatial resolution of about 0.6 mrad.

During the first years of operation a significant ageing of the HPC proportional chambers was observed, resulting in a progressive reduction in pulse-height. After four years of operation, a series of investigations were carried out using one of the modules of the HPC at the test beam facilities of the SPS, in 1993 and 1994. These investigations have shown that after a program of repairs and modified working conditions, the ageing in the readout proportional counters of the HPC does not significantly affect the detector performance and reliability until well after the end of the expected LEP data taking period (see **Publication III**).

3 Improvement of the Hermeticity

Tau physics, as well as many other physics topics, requires a hermetic detector for an accurate reconstruction of missing energy and momentum. There are several weak points in the DELPHI detector, where a significant portion of the energy can be lost. For example, the gaps between the barrel electromagnetic calorimeter (HPC) modules are about 1 cm in ϕ and z, except at θ = 90°, between the third and fourth rings, where there is a 7.5 cm gap to accomodate a stiffening ring for the cryostat. This central z-gap and the ϕ-gaps point straight back to the interaction region and make it possible for particles to escape undetected. The other z-gaps are much less serious but require some special care in shower reconstructions.

The largest gaps in the detector are in the region where the cable ducts between the barrel and the end caps are situated, creating rather large insensitive regions around θ = 40° and 140°.

To improve the hermeticity of the DELPHI detector, lead-scintillator counters were installed as described in the following. The counters cover the region with θ between 36° and 41° (and between 139° and 144°), which is 6.0% of the geometrical coverage of the DELPHI detector.

3.1 The 40° scintillator counters

There are three different types of lead-scintillator counters (referred to as *A, B* and *C* counters in the following) which have the same thickness but different shapes.

In 1994, 42 counters were installed on the **C** side of DELPHI ($\theta < 90°$) and in 1995 an additional 41 counters were installed on the **A** side ($\theta > 90°$) . These counters consist of a 2 cm thick lead absorber and a 1 cm thick scintillator.

The location of the counters in DELPHI is shown schematically in Fig. 3. The light is collected via 1 mm thick wavelength shifting fibers glued inside a grove, machined on the side of the scintillator. The light detector is a fine mesh PhotoMultiplier (Hamamatsu R5505) which can operate in the 1.2 T magnetic field of DELPHI with a typical gain of 10^4. Each pair of *B* and *C* counters were coupled directly to one PhotoMultiplier through an air gap, while the *A* counters were linked to the PhotoMultiplier with a one metre long fibre cable. Therefore the counters are referred to in the text as *BC* and *A* counters, The installation of the counters are explained in detail, in **Publication I**.

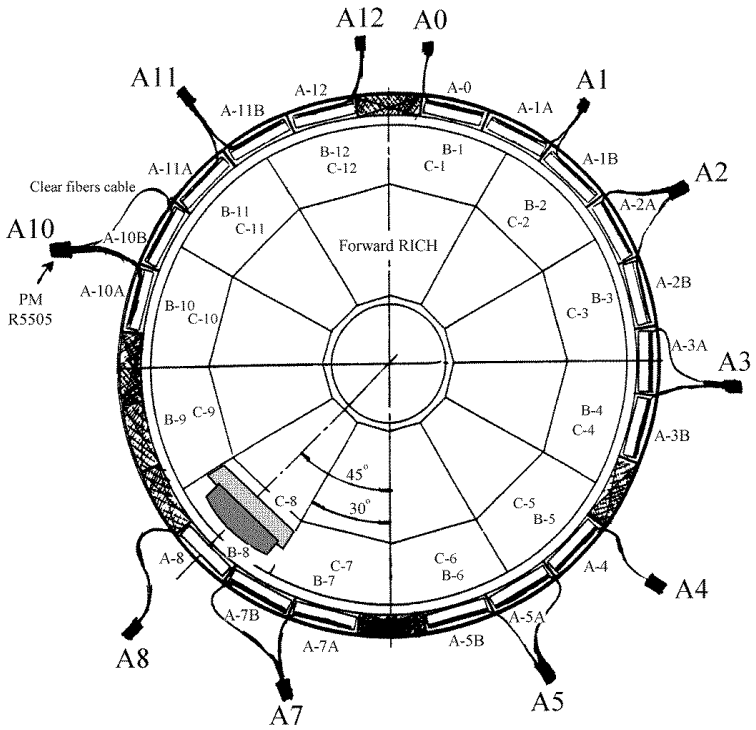

Figure 3: XY view of DELPHI C side with the counters position.

3.2 Testing the counters

In September 1994, the counters which were installed on the **C** side of DELPHI were tested in the X7 beam line of the SPS, to study the response of the counters to different energies. In order to study the effect of the field on the counter's performance some data were taken with a magnetic field, ranging up to 0.9 T. Data were collected with e^+ beams up to 20 GeV for each counter, and

the response to Minimum Ionizing Particles (MIP), was measured with data taken without the lead absorber.

The results of the test beam measurements are shown as MIP-equivalents [17], for different energies in Fig. 4. The number of MIP-equivalents is defined as the ratio between the peak position of the pulse height distribution from a counter, for a certain energy, with and without the lead. Since all the counters mounted in DELPHI have approximately the same light collection characteristics [17], the MIP-equivalent curves obtained are universal and can be used for calibration of the real data taken in DELPHI [18]. The test beam measurements of the scintillation counters are described in detail in **Publication II**.

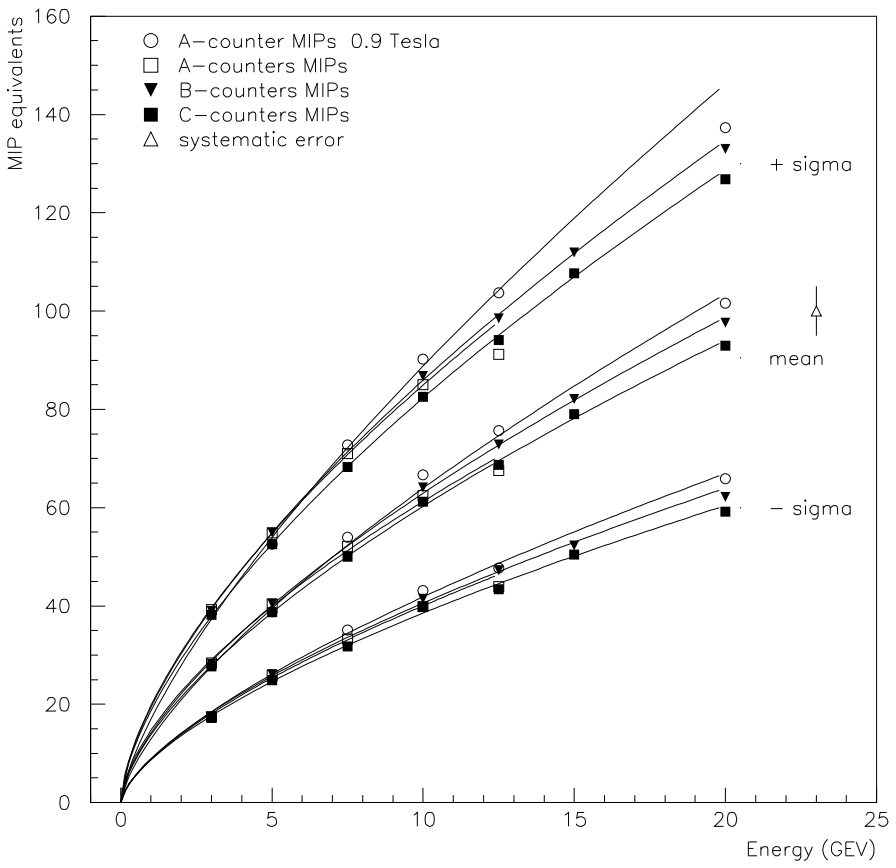

Figure 4: Test-beam results for the mean and $\pm$ 1 standard deviation points of the pulse height distribution (in MIP-equivalents) for the different counter types, plotted against the energy of the incoming positron. These results were obtained without magnetic field, except for the A-counters were the pulse heights corresponding to a magnetic field of 0.9 T are also shown.

3.3 The efficiency and Performance of the counters

After the installation of the counters on both sides of the DELPHI detector, they have been used in various physics analyses. The efficiency analysis of the counters with data taken in 1994 [19] shows that they improve the hermeticity of the detector. For muons the average detection efficiencies are 51.0 $\pm$ 1.8 $\%$ and 37.5 $\pm$ 2.5 $\%$ in the BC and A counters respectively. For high

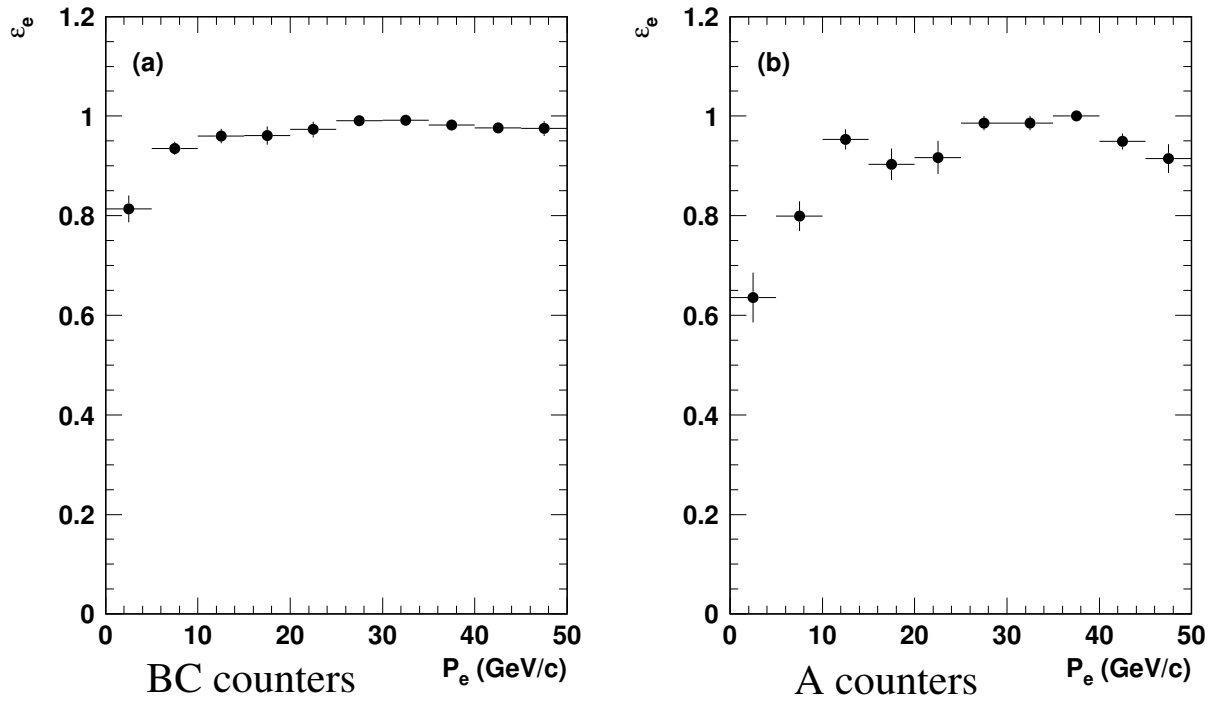

Figure 5: The efficiencies of the $40°$ counters calculated using the electrons from the data taken in 1994.

energy electrons the efficiency reaches 97.9 ± 0.4 % for the BC counters and 99.4 ± 0.3 % for the A counters (see Fig 5). Detecting muons in the counters as a function of their polar angle, gives a clear indication that the counters are covering this problematic region (see Fig 6).

The $40°$ counters are mainly used as 'veto counters' in new physics searches, as the search for supersymmetric particles (SUSY) [20] and for the Higgs boson [21]. These searches rely on a signature which is similar to the signature of the production of a Z boson where the initial state radiation photon is lost. This is particularly important for the second step of LEP (LEP2), where such photons often have high energies. The increased hermeticity achieved by the $40°$ counters is improving the efficiencies of these searches as well as other searches done at LEP1, at 91 GeV energy (see Fig 7).

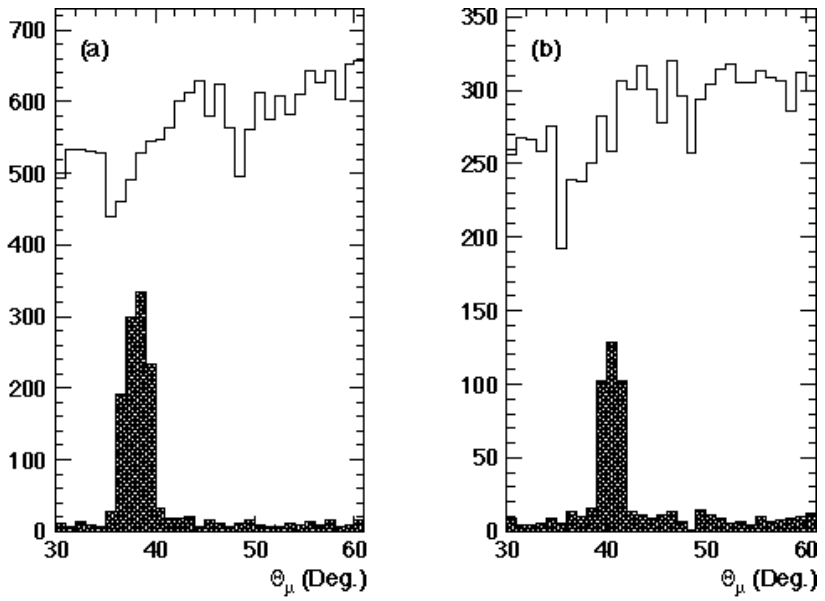

Figure 6: Polar angle distributions of muons detected in the *BC* (a) and *A* (b) counters. The open histograms show the selected muon candidates and the hatched histograms show the muons leaving a significant signal in the expected counter.

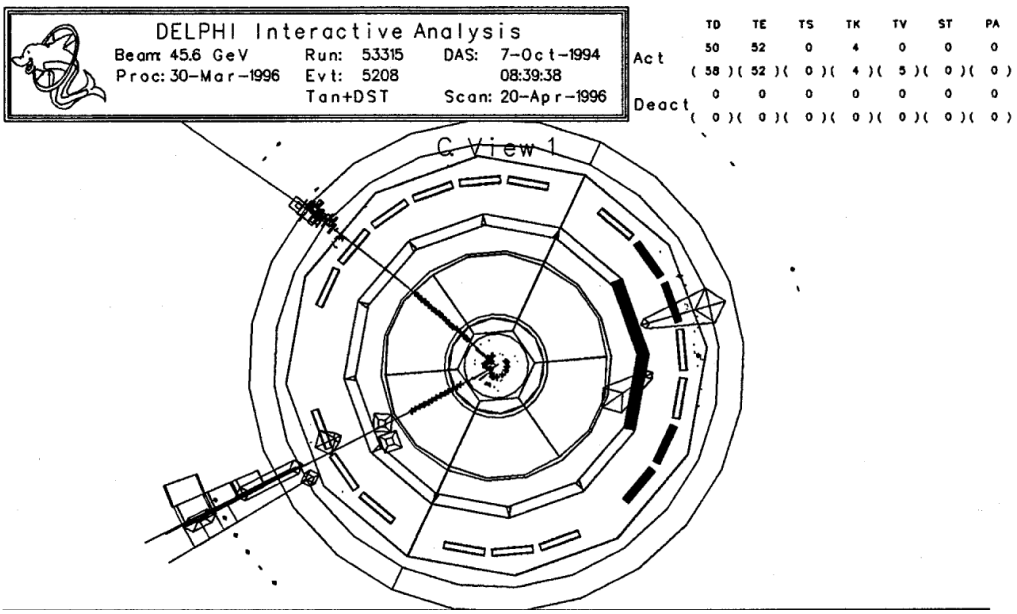

Figure 7: A "missing" photon in the $e^+e^- \to Z \to e^+e^-\gamma$ event is detected with the counters in the $40°$ region.

4 τ lepton physics

The tau lepton is a pointlike spin $\frac{1}{2}$ particle having a mass $m_\tau = 1777.1 \pm 0.4$ MeV and a lifetime $\tau_\tau = 296.6 \pm 3.1$fs [6].

In the minimal Standard Model [11], the τ lepton, together with its neutrino ν_τ form the third family of left-handed lepton doublets. The couplings of all families to the neutral and charged current are given by

- Neutral current :

$$\bar{l}\gamma_\mu(g_v^l - g_a^l\gamma_5)lZ_\mu \tag{1}$$

- Charged current :

$$\frac{g_{l\nu_l}^W}{2\sqrt{2}}\bar{\nu}_l\gamma_\mu(1-\gamma_5)lW_\mu^- \tag{2}$$

Figure 8: Couplings of the τ lepton to the neutral and charged current.

Here g_v^l, g_a^l are the vector and axial vector couplings of the lepton l to the neutral current :

$$g_v^l = \frac{-1}{2}(1 - 4sin^2\theta_W) \tag{3}$$

and

$$g_a^l = -\frac{1}{2} \tag{4}$$

where, $l = \tau, \mu, e$ and $sin^2\theta_W$ is the effective weak mixing angle. The universal coupling strength of the charged current $g_{l\nu_l}^W$ is related to the Fermi constant by:

$$G_F = \frac{(g_{l\nu_l}^W)^2}{4\sqrt{2}M_W^2} \tag{5}$$

The tau lepton decays via the W-emission diagram shown in Fig. 9. Since the W-coupling to the charged current is of universal strength, there are five equal contributions to the τ^- decay width (neglecting the final masses and gluonic corrections). Two of them are the decay modes $\tau^- \to \nu_\tau e^- \bar{\nu}_e$ and $\tau^- \to \nu_\tau \mu^- \bar{\nu}_\mu$, while the other three are the three possible colours of the quark-antiquark pair in the decay mode $\tau^- \to \nu_\tau d_\theta \bar{u}$, where $d_\theta = \cos\theta_c d + \sin\theta_c s$. Thus, the branching ratios for the different channels are:

$$B(\tau^- \to \nu_\tau e^- \bar{\nu_e}) = B(\tau^- \to \nu_\tau \mu^- \bar{\nu_\mu}) \approx \frac{1}{5} = 20\% \tag{6}$$

$$B_\tau = \frac{\Gamma(\tau^- \to \nu_\tau + hadrons)}{\Gamma(\tau^- \to \nu_\tau e^- \bar{\nu_e})} \approx N_c = 3 \tag{7}$$

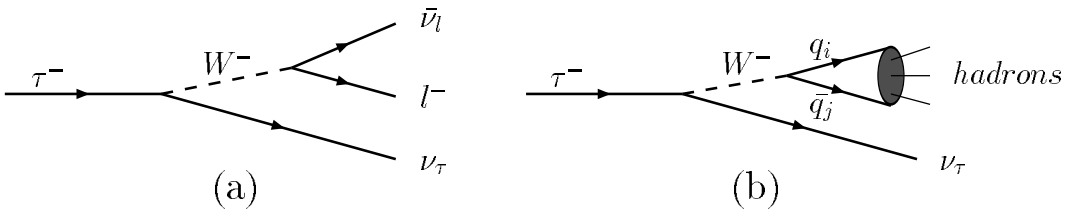

Figure 9: Feynman diagrams of the leptonic (a) and hadronic (b) decays of τ

4.1 τ production in $e^+e^- \to Z \to \tau^+\tau^-$

Approximately 3.3% of the Z bosons decay into $\tau^+\tau^-$ pairs. In this section, basic observables of tau physics at the Z pole in e^+e^- collision (shown in Fig. 10) are mentioned. The helicity conservation at high energy is one of the important concepts for the phenomenological properties of the $\tau^+\tau^-$ production. In quantum electrodynamics one writes,

$$\frac{(1-\gamma_5)}{2}u = u_L, \quad \frac{(1+\gamma_5)}{2}u = u_R \tag{8}$$

where u is the fermion spinor and γ_5 is the Dirac chirality operator. For a fermion with a large energy compared to its mass, the chirality states u_L and u_R correspond to the ± 1 helicity components of a spinor. In the annihilation of e^+e^-, the electron and the positron will always be found in states of opposite helicity: $e^+_R e^-_L$ or $e^+_L e^-_R$.

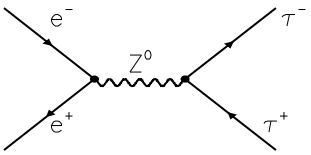

Figure 10: Feynman diagram of the process $e^+e^- \to Z \to \tau^+\tau^-$.

To identify the couplings of the chirality states we write:

$$g_v - g_a\gamma_5 = (g_v - g_a)\frac{(1+\gamma_5)}{2} + (g_v + g_a)\frac{(1-\gamma_5)}{2} = g_R\frac{(1+\gamma_5)}{2} + g_L\frac{(1-\gamma_5)}{2} \tag{9}$$

Hence $g_R \equiv (g_v - g_a)$, and $g_L \equiv (g_v + g_a)$ are the couplings of the right and left-handed components of a fermion spinor to the Z. Since $g_L \neq g_R$ the process will be parity violating. In the process $e^+e^- \to Z \to \tau^+\tau^-$, the taus have also opposite helicities $\tau^+_R\tau^-_L$ or $\tau^+_L\tau^-_R$, making

four allowed helicity configurations with $e^+_R e^-_L$ and $e^+_L e^-_R$. From the quantum mechanical theory of angular momentum, the amplitude is proportional to the rotation matrix element $d^j_{J_{z'},J_z}$, where J is the angular momentum and the z and z' axes are along the ingoing e^- and outgoing τ^- direction respectively [7]. There are four allowed helicity configurations and their corresponding amplitudes, like:

$$e^+_L e^-_R \to Z \to \tau^+_R \tau^-_L \Longrightarrow N_1 \propto (d^1_{-1,+1}(\theta)) g^e_R g^\tau_L \propto (1-\cos\theta) g^e_R g^\tau_L, ... \tag{10}$$

where g^e_R and g^τ_L are the coupling constants appropriate to the specific helicity configuration. Spin averaging the helicity amplitudes from N_1 to N_4, the differential cross-section is obtained:

$$\frac{d\sigma}{d\cos\theta} \propto 1 + \cos^2\theta + \frac{8}{3} A_{FB} \cos\theta \tag{11}$$

where

$$A_{FB} = \frac{3}{4} \frac{2 g^e_v g^e_a}{(g^e_v)^2 + (g^e_a)^2} \frac{2 g^\tau_v g^\tau_a}{(g^\tau_v)^2 + (g^\tau_a)^2} \tag{12}$$

Thus, experimentally an angular asymmetry will be observed by studying the cross-section for $e^+e^- \to Z \to \tau^+\tau^-$ as a function of $\cos\theta$. The observable A_{FB} is known as the forward-backward asymmetry.

The different strengths of the couplings of the Z boson to the right-handed and left-handed e^+ and e^- induce a polarization to Z and to τ. The mean tau polarization is given in the improved Born approximation as [8] :

$$\langle P_{\tau -} \rangle = -\frac{2 g^\tau_v g^\tau_a}{(g^\tau_v)^2 + (g^\tau_a)^2} \tag{13}$$

The polarization of the Z boson induces a dependence of $P_{\tau -}$ on the polar angle θ of the τ^- production relative to the incident e^- beam. This gives an observable:

$$P_{\tau -}(\cos\theta) = \frac{N^+_{\tau -}(\cos\theta) - N^-_{\tau -}(\cos\theta)}{N^+_{\tau -}(\cos\theta) + N^-_{\tau -}(\cos\theta)} = \frac{\langle P_{\tau -} \rangle (1+\cos^2\theta) + \langle P_{e -} \rangle (2\cos\theta)}{(1+\cos^2\theta) + 2\langle P_{\tau -} \rangle \langle P_{e -} \rangle (2\cos\theta)} \tag{14}$$

where $N^\pm_{\tau -}(\cos\theta)$ is the number of τ^- produced at a given $\cos\theta$ with helicity ± 1 and $\langle P_{e -} \rangle$ is the electron polarization obtained by substituting in expression (13) all the τ^- coupling constants with the e^- coupling constants. The last part of expression (14) is derived using the equations (10) and (13). In the Standard Model of electroweak interactions, the coupling constants g_v and g_a for leptons are related to the mixing angle $\sin^2\theta_W$ through the equations (3) and (4). Introducing them in (12) and (13), one obtains:

$$\langle P_{\tau -} \rangle \approx -2(1 - 4\sin^2\theta_W) \tag{15}$$

and

$$A_{FB} \approx 3(1 - 8\sin^2\theta_W + 16(\sin^2\theta_W)^2) \tag{16}$$

Thus, the measurement of P_τ and A_{FB} can provide information on the electroweak parameter $\sin^2\theta_W$. From the measurements of the τ polarization from 1991 and 1992 data taken in DELPHI, the ratio of vector to axial-vector effective couplings for taus $g^\tau_v/g^\tau_a = 0.074 \pm 0.011$ is obtained, implying a value of the effective weak mixing angle $\sin^2\theta_W = 0.2320 \pm 0.0021$ [22].

The other important observables of tau physics, are the branching ratios of τ decays. Measurements of inclusive τ decay rates can be used to determine the value of the QCD running coupling $\alpha_s(m_\tau^2)$ at the scale of the τ mass. The result can then be evolved to the Z mass scale, $\alpha_s(m_Z^2)$. The ratio of the total hadronic and the leptonic decay widths of the τ, defined by:

$$R_\tau = \frac{\Gamma(\tau \to hadrons\ \nu_\tau)}{\Gamma(\tau \to l\nu_\tau\bar{\nu}_l)} \tag{17}$$

can be calculated from the measured leptonic branching ratios:

$$R_\tau = \frac{1 - B_e - B_\mu}{B_l} \tag{18}$$

where B_e and B_μ are the electron and muon branching ratios of tau decay respectively, while B_l is the total leptonic branching ratio. The perturbative QCD correction to R_τ has been calculated to third order in α_s [13]. Using these calculations and the measured value of R_τ, the strong coupling constant is measured to be $\alpha_s(m_\tau) = 0.26^{+0.009}_{-0.12}$ in DELPHI [22].

Tau physics at LEP, also gives a tool for testing the lepton universality in the Standard Model, by measuring the ratio

$$\left(\frac{G_\tau}{G_\mu}\right)^2 = \left(\frac{\tau_\mu}{\tau_\tau}\right)\left(\frac{M_\mu}{M_\tau}\right)^5 B(\tau \to e\nu\bar{\nu}) \tag{19}$$

where G_τ and G_μ, the Fermi coupling constants of the τ and μ to the charged weak current, are equal in the Standard Model. From the data taken in DELPHI in 1991 [10] and in 1992 [5], the ratios of the couplings to the weak charged current are measured to be $G_\tau/G_\mu = 0.985 \pm 0.013$ and $G_\mu/G_e = 1.000 \pm 0.013$ respectively, satisfying lepton universality.

5 Selection of $\tau^+\tau^-$ events in DELPHI

At the Z peak, a $\tau^+\tau^-$ event is characterized by two low-multiplicity, back-to-back jets of particles, where the neutrinos coming from the τ decays will result in a significant missing energy. A $\tau^+\tau^-$ event where the taus decayed to an electron and a muon respectively is shown in Fig. 11. The background from multihadron production at LEP energies can easily be reduced since it is characterized by a relatively high charged multiplicity. Backgrounds from $e^+e^- \to e^+e^-$ and $e^+e^- \to \mu^+\mu^-$ leave very characteristic signatures in DELPHI. Radiative events, $e^+e^- \to e^+e^-\gamma$ and $e^+e^- \to \mu^+\mu^-\gamma$ can also be correctly identified due to the good hermeticity of the calorimetry. Two-photon collisions, $e^+e^- \to e^+e^-X$, are also easily identified and removed from the $\tau^+\tau^-$ event sample, due to their high acolinearity. As a consequence, high purity τ samples can be attained in DELPHI.

5.1 Event Selection

The selection criteria for tau pairs are documented in [15] and will be described in the following. To ensure a good detector response, in this analysis it is required that the subdetectors VD,TPC and HPC are fully operational and the event is contained in the barrel region of the DELPHI detector.

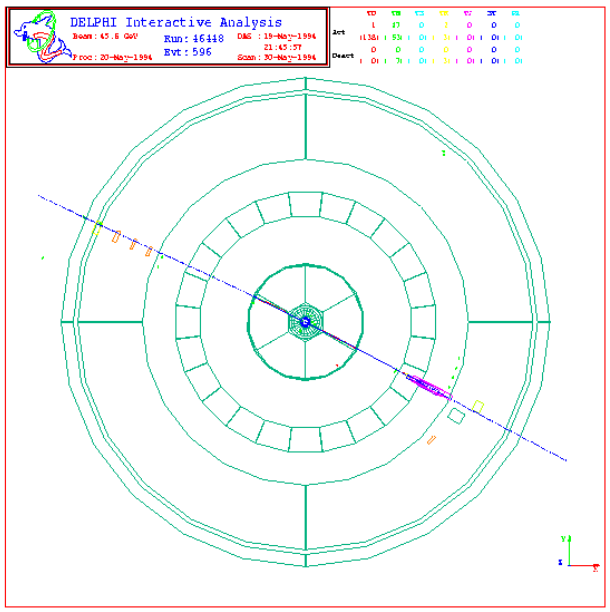

Figure 11: $\tau^+\tau^-$ event, where one of the taus in one hemisphere decays to an electron and the other one decay to a muon in the other hemisphere, seen on the DELPHI interactive analysis display.

Each event is divided into hemispheres by a plane perpendicular to the thrust axis, which is calculated using the charged particles. The highest momentum charged particle in each hemisphere is defined as the leading particle for that hemisphere. At least one of the two leading particles per event is required to lie in the barrel region of the detector ($43° < \theta < 137°$). This cut will be referred to in the following as the "geometric acceptance cut". All energy deposited in the electromagnetic calorimeters within $30°$ of the leading track is defined as its 'calorimetric energy'. A fiducial region is defined around the interaction point (5 cm in r and 10 cm in z), and charged tracks only from this region are accepted. Events with more than six reconstructed charged tracks are rejected.

To remove $q\,\bar{q}$ and $\gamma\gamma$ events, it is required that:

- $\theta_{iso} \geq 160°$
- $E_{vis} > 8$ GeV
- $2 \leq N_{chr} \leq 6$

where θ_{iso} is the minimum angle between any pair of tracks belonging to opposite hemispheres, the visible energy E_{vis} is the scalar sum of momenta of the charged particles added to the total neutral electromagnetic energy, N_{chr} is the number of charged tracks in the event.

To reject beam gas events and leptonic final states from Z decays it is required that:

- $\mid z_{1,2} \mid < 4.5$ cm
- $\mid d_{1,2} \mid < 1.5$ cm

- $P_{rad} = \sqrt{\frac{P_1^2+P_2^2}{E_{beam}}} < 1$
- $E_{rad} = \sqrt{\frac{E_1^2+E_2^2}{E_{beam}}} < 1$

where P_i and E_i are the momentum and the total electromagnetic energy of the leading particle in hemisphere i. The cut variables d_i and z_i are defined as the transverse and longitudinal distances of closest approach to the interaction point for the leading tracks. Finally, to reduce further the contamination for events with two charged tracks it is required that these obey the following criteria:

- $P_T^{miss} > 0.4$ cm
- $\theta_{acol} > 0.5°$
- $\mid z_1 - z_2 \mid < 3.0$ cm

where P_T^{miss} is the transverse component of the total momentum of the event, and θ_{acol} is the acollinearity angle. The acollinearity cut removes $Z \to \mu^+\mu^-$ and Bhabha events, whereas the cut on P_T^{miss} rejects two-photon interactions. The cut on the longitudinal distances of closest approach to the average beam spot (z_i) for the leading tracks reduces the cosmic background. In Figs. 12, 13 and 14 the distributions of some of these variables are shown for real and simulated events.

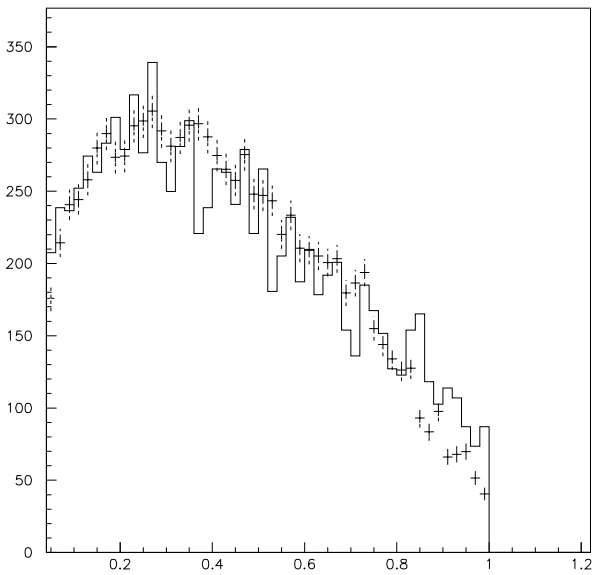

Figure 12: E_{rad} distribution of Monte Carlo simulation superimposed on data.

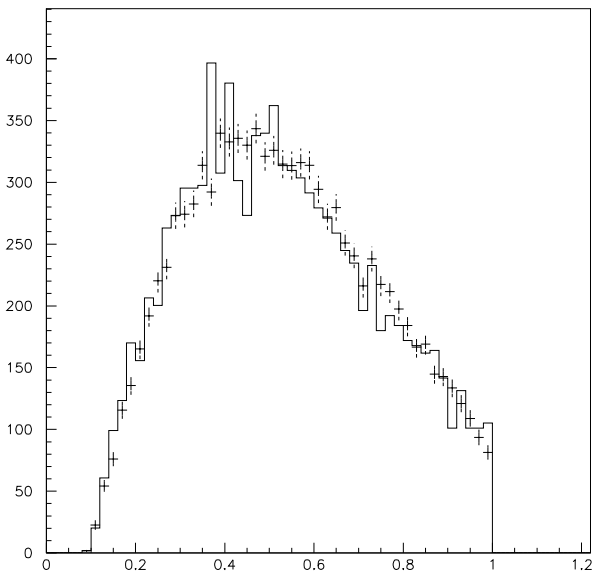

Figure 13: P_{rad} distribution of Monte Carlo simulation superimposed on data.

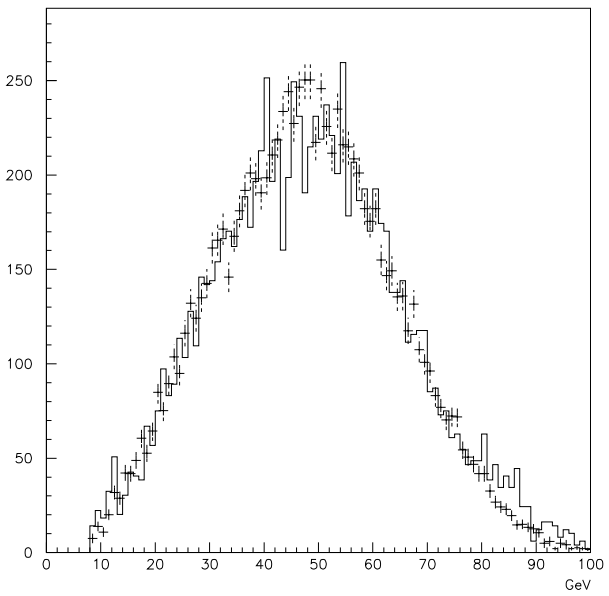

Figure 14: Visible energy E_{vis} distribution of Monte Carlo simulation superimposed on data.

5.1.1 Selection Efficiency

To determine the detection efficiency $e^+e^- \rightarrow Z \rightarrow \tau^+\tau^-$ events were generated using the KORALZ [24] program. The events were then processed through a detailed simulation and reconstructed by the same program as the real data, applying the same selection criteria. The geometrical acceptance, as defined by the acceptance cut defined above and calculated from the total generated tau sample is $50.1 \pm 0.6\%$. Inside the geometrical acceptance (barrel region), the efficiency reaches $69.3 \pm 0.5\%$. The overall efficiency and the efficiency inside the geometrical acceptance are shown in Fig. 15 for the "true topologies" 1-1,1-3, 1-5 and 3-3.

The overall efficiencies and the efficiencies inside the geometrical acceptance do not follow the same pattern for different topologies. Due to this effect, the branching ratios are not the same in the region defined by the acceptance cut, and they have to be corrected with a bias factor as explained in chapter 6.

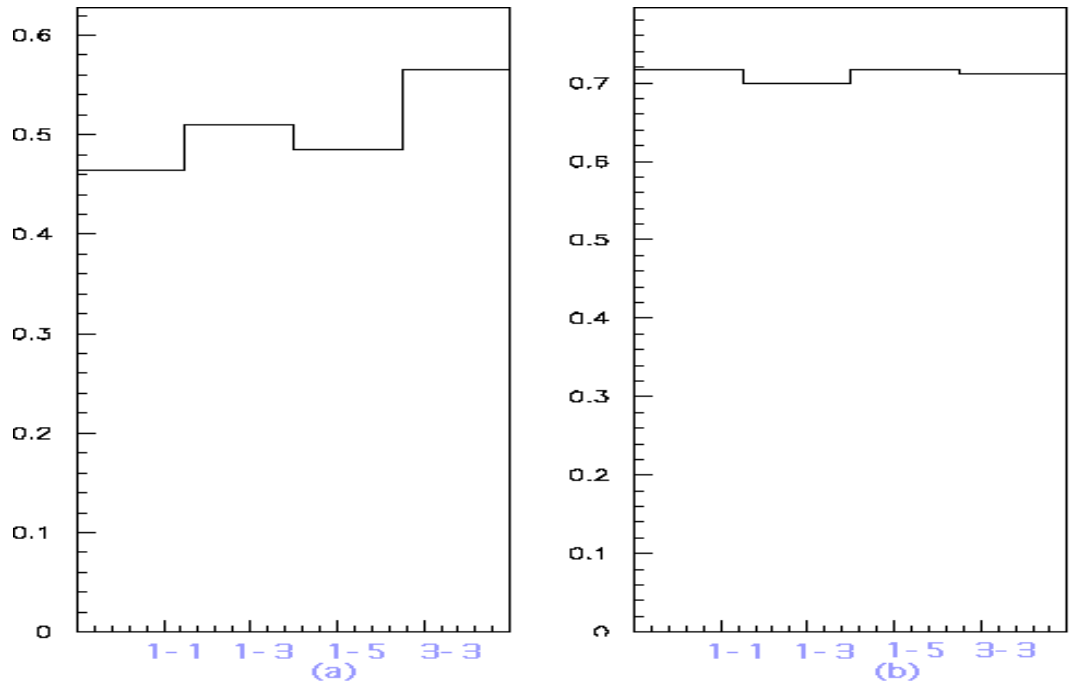

Figure 15: Overall efficiencies calculated from all the $Z \rightarrow \tau^+\tau^-$ events (a), and the efficiencies for events in the barrel region defined by the geometrical acceptance (b), for the 'true topologies' of $\tau^+\tau^-$ decays (1-1 , 1-3, 1-5, 3-3).

5.1.2 Background

For the background studies, events with e^+e^- final states are produced with BABAMC [25], $\mu^+\mu^-$ final states with DYMU3 [26] and hadronic final states with JETSET 7.3 [27]. The same τ selection criteria are applied to the background events. The background for high multiplicity decays of the τ are dominated by hadronic decays of Z and two-photon interactions. In the low multiplicity decays the main background are e^+e^- and $\mu^+\mu^-$ events. The backgrounds for different topologies are shown in Fig. 16 and in table 2.

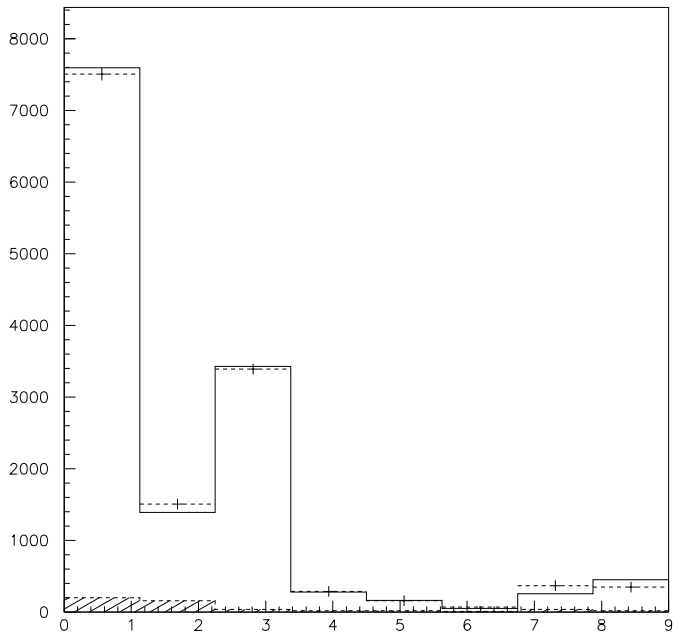

Figure 16: Expected topologies 1-1,1-2,1-3,1-4,1-5,2-2,2-3 and 3-3 of the $\tau^+\tau^-$ events in simulation (solid) calculated according to the equation (25), and the observed topologies (dashed) in data. The hatched areas show the background contribution.

6 Migration of Topologies

Tau pairs are easily separated by dividing the event in two hemispheres with a plane perpendicular to the thrust axis determined from charged particles. Each tau particle in a $\tau^+\tau^-$ event, decays to an odd number of charged particles. The event topology is then defined as i-j , where i and j are the number of charged particles in each hemisphere, with i,j = 1,3,5 . The event appears in the detector with a possibly different topology k-l , where k,l=1,2,3,4,5... , due to secondary interactions, inefficient regions for track reconstruction, inefficiencies of the pattern recognition algorithms and detector resolutions. The 'reconstructed' (observed) event topology becomes 1-1, 1-2, 1-3, 1-4, 1-5, 2-2, 2-3 or 3-3. The possibility to observe a topology i-j as k-l is described by the migration matrix $P_{ij\to kl}$ which is obtained from the simulation (see table 1). This gives us:

$$n_{kl} = \sum_{ij} P_{ij\to kl} N_{ij} \tag{20}$$

where n_{kl} is the number of expected events after migration and N_{ij} is the number of events produced in 'true' topologies (generated events, before entering the detector). Accounting for background and detection efficiency of each topology, the expected number of events from the detector is found as:

$$m_{kl} = m_{kl}^{bg} + \epsilon_{kl} \cdot n_{kl} \tag{21}$$

where, ϵ_{kl} is the detection efficiency of the k-l topology event, inside the geometrical acceptance.

The inclusive branching ratios (B_i) of the τ decay final states are related to the number of events in true topologies (N_{ij}) :

$$N_{ij} = (2 - \delta_{ij}) \cdot N_{\tau\tau} \cdot B_i \cdot B_j \tag{22}$$

where B_i is the branching ratio of a tau decaying into i charged particles, inside the acceptance region, and $N_{\tau\tau}$ is the number of $\tau^+\tau^-$ events.

The expected number of events for each topology becomes:

$$m_{kl} = m_{kl}^{bg} + \epsilon_{kl} \cdot \sum_{ij} P_{ij\to kl}(2 - \delta_{ij}) \cdot N_{\tau\tau} \cdot B_i \cdot B_j \tag{23}$$

But these branching ratios (B_i) have to be corrected with a bias factor, due to the fact that they are not the same inside the acceptance region. For the correction, the bias factor BS_{ij} can be defined as:

$$BS_{ij} = \frac{(B_i Bj)^{inside}}{(B_i Bj)^{total}} = \frac{N_{\tau\tau}^{total} N_{ij}^{inside}}{N_{\tau\tau}^{inside} N_{ij}^{total}} \tag{24}$$

Inserting the bias factor calculated from the equation (24) into (23) one obtains the final expression for the expected number of events for the topologies k-l.

$$m_{kl} = m_{kl}^{bg} + \epsilon_{kl} \cdot \sum_{ij} P_{ij\to kl}(2 - \delta_{ij}) \cdot N_{\tau\tau} \cdot BS_{ij} \cdot B_i \cdot B_j \tag{25}$$

In chapter 9, this expression for the number of expected events m_{kl} for each topology k-l, will be fitted to the observed number of events from the data and thus to calculate the topological branching ratios B_i's. (see Table 3).

Topology	1-1	1-3	1-5	3-3
1-1	82.90 $\pm$0.73	0.93 $\pm$0.12	0.00 $\pm$0.00	0.00 $\pm$0.00
1-2	7.90 $\pm$0.22	13.89 $\pm$0.46	4.92 $\pm$2.84	1.02 $\pm$0.39
1-3	7.12 $\pm$0.21	69.67 $\pm$1.03	16.39 $\pm$5.18	2.04 $\pm$0.55
1-4	0.70 $\pm$0.07	3.91 $\pm$0.24	36.07 $\pm$7.69	0.44 $\pm$0.25
1-5	0.26 $\pm$0.04	1.95 $\pm$0.17	32.79 $\pm$7.33	0.15 $\pm$0.15
2-2	0.13 $\pm$0.03	0.68 $\pm$0.10	0.00 $\pm$0.00	3.21 $\pm$0.68
2-3	0.27 $\pm$0.04	3.45 $\pm$0.23	0.00 $\pm$0.00	21.75 $\pm$1.78
3-3	0.24 $\pm$ 0.04	4.23 $\pm$0.25	1.64 $\pm$1.64	65.40 $\pm$3.09

Table 1: Migration matrix, where the "true topologies" 1-1, 1-3, 1-5 and 3-3 are observed as 1-1, 1-2, 1-3, 1-4, 1-5, 2-2, 2-3 and 3-3.

7 Comparison of the Migration Matrix

As seen from the table 1, the migration matrix is not diagonal. Ideally, this matrix should be diagonal, and in many measurements of the topological branching ratio measurements attempts

have been made to make it more diagonal. In this analysis, we will not try to make the migration matrix diagonal, but rather to understand it. In other words, as far as our simulation of the migration is correct, we can trust our values of the branching ratios. The only way to check the migration matrix is to compare event characteristics in real and simulated data. Since we do not know the migration of the real data, we try to fit each topology to the real data using the distributions of the well know topologies from the simulation. The most problematic one, is the 1-2 topology. In the fit of eq. (25) to the number of observed events, the chi-square contribution for the 1-2 topology is much larger than for any other (see table 3). In simulation, 55.4% of the 1-2 events come from the 1-1 topology, and 44.6% of them come from the 1-3 topology. To check the same ratio in real data, we fitted momentum distributions (e.g. for the most energetic or second most energetic particle) of the 1-1$\rightarrow$ 1-2 events and 1-3$\rightarrow$ 1-2 events in the simulation, to the same distributions of the x-x$\rightarrow$ 1-2 events in the real data.

$$R(p)_{x-x\rightarrow 1-2} = aO(p)_{1-1\rightarrow 1-2} + bT(p)_{1-3\rightarrow 1-2} \tag{26}$$

where $O(p)_{1-1\rightarrow 1-2}$ and $T(p)_{1-3\rightarrow 1-2}$ are the distributions of the 1-1$\rightarrow$ 1-2 and 1-3$\rightarrow$ 1-2 events obtained from the simulation, whereas $R(p)_{x-x\rightarrow 1-2}$ is the same distribution from the real data normalized to the simulation (see Fig. 17). These different fits gave similar results. The result of the momentum distribution for from the second most energetic particle is:

- a = 48.7 $\pm$ 0.4 $\%$ (1-2 topology events coming from 1-1 topology)
- b = 51.3 $\pm$ 0.4 $\%$ (1-2 topology events coming from 1-3 topology)

This shows us that we have slightly more 1-2 topology events coming from 1-3 topology events in real data than in simulations.

8 Reconstruction problems and corrections

To get better agreement between the simulation and the real data various methods have been used in other analyses [28, 29]. All these correction methods are mainly based on the removal of photon conversions and corrections to the track reconstruction. The problem with these methods is that they do not always give the same result for data and simulation. In this analysis it is found that the main problem in calculating the branching ratios is the 1-2 topology events. They are not one of the 'true topologies' and they are numerous (see table 3). Since the χ^2 contribution of these 1-2 topology events is very high, any correction to get a better agreement between the simulation and the real data should concentrate on those events. An example of this kind of events is shown in Fig. 18. From the fit explained in chapter 7, 1-3 events contribute more to 1-2 events in data than in simulation. This effect has to be corrected either in the simulation of the DELPHI detector or in the real data in such a way that the migration matrix of the simulation agrees with the real data.

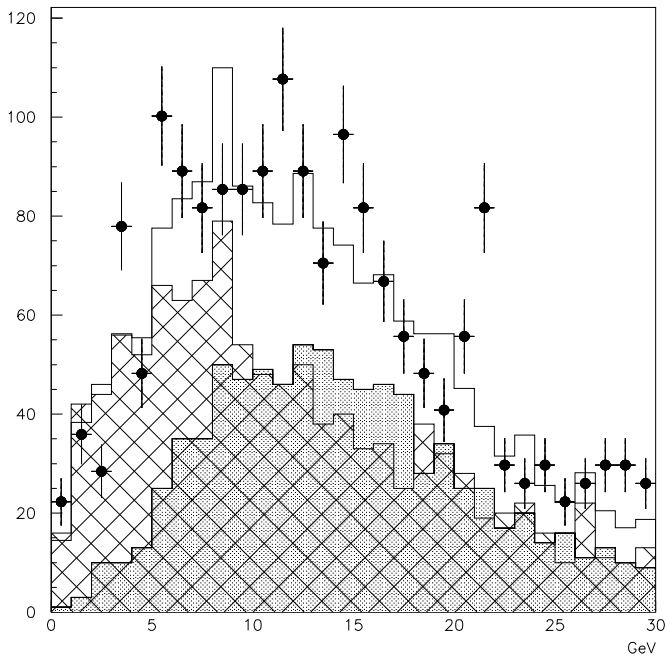

Figure 17: Second most energetic particle momentum distribution for the 1-2 topology events in real data (dots) superimposed with the same distribution of the "corrected" 1-2 events obtained in simulation, after the fit described in chapter 7. In the simulation there are two cases: 1-2 topology events coming from the 1-1 topology events (hatched) and 1-2 topology events coming from the 1-3 events (grey hatched). The distributions for these topologies are normalized with the factors *a* and *b* respectively and summed together (open histogram).

9 The Inclusive branching Ratio Measurements

Fitting the expected number of events m_{kl} to the observed number of events with the least squares method, we obtained the values for branching ratios as:

$$B_1 = 84.38 \pm 0.27 \pm 0.35\%$$
$$B_3 = 14.90 \pm 0.27 \pm 0.23\%$$
$$B_5 = 0.51 \pm 0.12 \pm 0.11\%$$

where the first error is statistical and the second is systematic. In this fit $N_{\tau\tau}$ is fixed to the value computed from the luminosity. The maximum likelihood method has also been used for a consistency check, giving no significant difference. The total χ^2 per degree of freedom of the fit is 13.99/5= 2.79, implying a χ^2 probability of 1.6 %. This is mainly due to the contribution of 1-2 topology events that we discussed in chapter 7.

The systematic effects due to the selection cuts have been calculated by estimating the uncertainty on the measurement of each variable used for the cuts and varying the cut value by one standard deviation up and down.

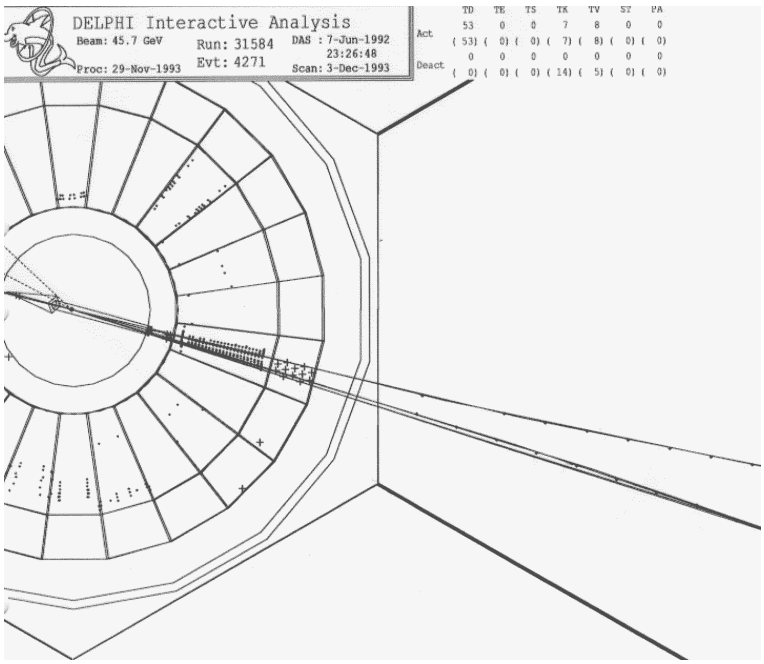

Figure 18: Originally 1-3 topology event reconstructed as a 1-2 topology event at the detector, as seen on the DELPHI interactive analysis display. Due to the poor detector resolution, one of the three charged tracks in one hemisphere is lost, and only two charged tracks are reconstructed.

Topology	Bias Factor	Geometrical Efficiency (%)
1-1	0.993 $\pm$0.004	71.7 $\pm$0.3
1-3	1.018 $\pm$0.003	70.0 $\pm$0.4
1-5	0.994 $\pm$0.002	71.6 $\pm$0.3
3-3	0.999 $\pm$0.002	71.2 $\pm$0.5

Table 2: Bias factor and efficiencies for the true topologies.

10 Conclusion

As described above, in this analysis, the simulation plays a crucial rôle. To have a reliable result, one has to have a good agreement between the real data and the simulation of the physical processes.The biggest chi-square contribution to our fit comes from the 1-2 event topology (one charged particle in one hemisphere and 2 charged particle in the other hemisphere), where we have more 1-2 topology events in data than expected. Apparently, the migration matrix is different for real data. Although the χ^2 contribution for this channel is quite high, a reasonable agreement is obtained with the results from other measurements [28, 30] and the Particle Data Group [6] (see table 4).

Topology	Observed events	Expected events	χ^2	Efficiency (%)	Background (%)
1-1	9050	9145.18	0.932	65.4 ± 0.5	2.68
1-2	1818	1689.32	6.444	70.2 ± 0.4	10.61
1-3	4090	4127.04	0.358	78.3 ± 0.3	1.15
1-4	349	345.29	0.146	67.1 ± 0.4	6.92
1-5	192	194.36	0.063	63.0 ± 0.4	12.58
2-2	87	69.32	3.721	66.2 ± 0.5	16.67
2-3	446	426.35	1.502	74.3 ± 0.5	10.81
3-3	422	431.00	0.823	84.8 ± 0.4	5.71

Table 3: Observed and expected number of events,chi-square contribution of the fit, efficiencies and the background for each topology.

Branching Ratios (%)	DELPHI 1992	PDG 1994	M. de Fez-Laso (1994)
B_1 (1 charged p.)	84.38±0.27±0.35	85.49±0.24	85.26±0.23±0.15
B_3 (3 charged p.)	14.90±0.27±0.23	14.38±0.24	14.37±0.24±0.16
B_5 (5 charged p.)	0.51±0.12±0.11	0.12±0.02	0.37±0.10±0.06

Table 4: The measured topological branching ratios of the tau lepton compaired with the world average and with another DELPHI analysis.

Acknowledgments

I am greatly indebted to all members of the Particle Physics group in Stockholm. Many thanks to Prof. Sven-Olof Holmgren who has encouraged and supported me as well as being engaged in long fruitful discussions. Many thanks to my supervisor Doc. Klas Hultqvist who supplied fruitful comments. I would also like to express my gratitude to Doc. Christian Walck who shared his vast knowledge of statistics with me. Many thanks also to Prof. P.O. Hulth for his support over the years.
Working in big experiment like DELPHI has been a fascinating experience. I would like to thank Dr Alberto Benvenuti whom I enjoyed very much to work with. I am also greatly indebted to my collaborators and to the funding agencies for their support in building and operating the DELPHI detector, and to all people working at LEP for the excellent quality of their work.

References

[1] M. L. Perl et al., Phys. Rev. Lett. 35, *(1975) 1489.*

[2] H. Albrecht et al., ARGUS collab., *Zeit. Phys.* **C53** (1992)367.

[3] P. Privitera , *A Measurement of the τ mass*, Delphi note 93-58 PHYS 286, 16 June 1993.

[4] DELPHI Collaboration, P. Abreu et al., *A Precise Measurement of the Tau Lepton Lifetime.* Phys. Lett. **B365** (1996) 448.

[5] DELPHI Collaboration, P. Abreu et al., *A Measurement of the Tau leptonic branching fractions.* Phys. Letters. **B 357** (1995) 715.

[6] Particle Data Group, *Review of Particle Properties*, Phys.Rev. **D54**, (1996) 1.

[7] Halzen, F., D. Martin A., *Quarks & Leptons*, John Wiley & Sons, (1984).

[8] Z Physics at LEP I, edited by G. Altarelli, R. Kleiss and C. Verzegnassi, CERN 89-08 (1989).

[9] DELPHI Collaboration, P. Abreu et al., *Measurements of the Tau Polarization in Z° decays.* Zeit. Phys. **C67** (1995) 183.

[10] DELPHI Collaboration, P. Abreu et al., *A Measurement of the Tau Lifetime*, Phys. Letters. **B302** (1993) 356, 25 March 1993.

[11] S.L. Glashow, *Nucl. Phys.* **22** (1967)579.

S. Weinberg, *Phys. Rev. Lett.* **19** (1967)1264.

M. Gell-Mann, *Acta Physica Austriaca, Suppl.* **IX** (1072)733.

G. Altarelli, Phys. Rep. **81** (1982)1.

[12] DELPHI Collaboration, P.Aarnio et al., *The DELPHI Detector at LEP* Nucl.Instr.& Meth. **A303** (1991) 233.

[13] E. Braaten, S. Narison and A. Pich, Nucl.Instr.& Meth. **B373** (1992) 581.

[14] DELPHI Collaboration, P. Abreu et al., *Performance of the DELPHI Detector* Nucl. Phys. **A378** (1996) 57–100, 11 August 1995.

[15] DELPHI Collaboration, F. Matorras, *DELPHI 92-124 PHYS 225*, 9-SEP-92.

[16] Bell, W., Bonivento, W., Cankoçak, K., Cattai, A., Contri, R., De Min, A., Gorn, L., Navarria, F.L., Ragazzi, S., Szczekowsky, M., Tabarelli de Fatis, T. and Tonazzo, A., *Performance of an artificially aged module of the DELPHI HPC calorimeter*, Nucl.Instr.& Meth. **A378**, (1996) 499.

[17] P. Bambade, A. Benvenuti, M. Boldini, B. Buisson, K. Cankoçak, G. Dubois Dauphin, Ch. De La Vaissiere, V. Giordano, P. Gunnarsson, D. Imbault, A. Jouenne, F. Kapusta, P. Laloux, J. Lesueur, L. Maselli, A. Morelli, P. Rebecchi, M. Rebut, J. Renaud, K. Truong, *Test and Installation of the 40^o Counters during the 1993/1994 Shut Down*, DELPHI note 94-48 HERM 1, 5 May 1994.

[18] K. Cankoçak, P. Andersson, A. Benvenuti, P. Rebecchi, S. Holmgren, *Study of the* 40^{o} *Counters in a test beam 1993/1994 Shut Down*, DELPHI note 95-152 CAL-127, 3 Oct 1995.

[19] F. Stichelbaut , *Study of the Performance of the* 40° *Counters with 94 Data*, DELPHI note 96-18 HERM-2, 22 Feb 1996.

[20] P. Rebecchi, *Ph. D. thesis*, Universite De Paris Sud Centre D'Orsay **LAL 96-30**, May 1996.

DELPHI Collaboration: P. Abreu et al., *Search for the Lightest Chargino at* $\sqrt{s} = 130$ *and 136 GeV*, Physics Letters **B382** (1996) 323, 8 August 1996.

DELPHI Collaboration: : P. Abreu et al., *Search for neutralinos, scalar leptons and scalar quarks in* $\mathrm{e^+e^-}$ *interactions at* $\sqrt{s} = 130$ *GeV and 136 GeV*, Physics Letters **B387** (1996) 651, 24 October 1996.

DELPHI Collaboration: P. Abreu et al., *Search for Charginos, Neutralinos and Gravitinos at LEP*, European Phys. J. **C1** (1998) 1-20 , January 1998.

[21] DELPHI Collaboration: P. Abreu et al., *Search for Neutral and Charged Higgs Bosons in* $\mathrm{e^+e^-}$ *Collisions at* $\sqrt{s}$*=161 GeV and 172 GeV*, CERN-PPE/97-085, 17 July 1997.

[22] DELPHI Collaboration: P. Abreu et al., *A Study of the Decays of Tau Leptons Produced on the* Z *Resonance at LEP*, Physics Letters **B291** (1992) 503, September 1992.

[23] DELPHI Collaboration: P. Abreu et al., *Measurements of the Lineshape of the* Z^{o} *and Determination of Electroweak Parameters from its Hadronic and Leptonic Decays*, Nuclear Physics **B417** (1994) 3–57, 11 April 1994; erratum *ibid* **B426** (1994) 244.

[24] S. Jadach and Z. Was, *Comp. Phys. Commun.* **36**, (1985) 191.

[25] F. A. berends, W. Hollik and R. Kleiss, *Nucl. Phys.* **B304**, (1988) 712.

[26] J. E. Campagne and R. Zitoun, *Zeit. Phys.* **C43**, (1989) 469.

[27] T. Sjöstrand, *Comp. Phys. Commun.* **39**, (1986) 347.

[28] M. de Fez-Laso, J.J. Gomez-Cadenas, *DELPHI 94-140 PHYS 449*, September 21, 1994.

[29] DELPHI Collaboration, *Measurement of the charged particle multiplicity in* τ *decays*, DELPHI note PHYS 212, 92-106, Rochester Conference, Dallas, 1992.

[30] OPAL Collaboration: P. D. Acton et al., *Measurement of the* τ *Topological Branching Ratios at LEP*, Physics Letters **B288** (1992) 373, 27 August 1992.

L3 Collaboration: B. Adeva et al., *Decay Properties of Tau Leptons Measured at the* Z^{0} *Resonance*, Physics Letters **B265** (1991) 451, 15 August 1991.

ALEPH Collaboration: D. Decamp et al., *Measurement of Tau Branching Ratios*, Z. Phys. **C54** (1992) 211–228, May 1992